

The Volcanic History of Syria Planum, Mars

Jacob A. Richardson^{a,*}, Jacob E. Bleacher^b, Lori S. Glaze^b

^a*University of South Florida, Department of Geology, Tampa, FL, United States*

^b*NASA Goddard Space Flight Center, Planetary Geodynamics Lab, Greenbelt, MD, United States*

Abstract

A field of small (10s km in diameter) volcanoes in the Syria Planum region of Mars is mapped to determine abundance, distribution, and alignments of vents. These data are used to assess possible variations in eruption style across space and time. Each eruption site is assigned a point location. Nearest neighbor and two-point azimuth analyses are conducted to assess the spacing and orientations between vents across the study area. Two vent fields are identified as unique volcanic units along with the previously identified Syria Mons volcano. Superposition relationships and crater counts indicate that these three volcanic episodes span \sim 900 Ma, beginning in the early Hesperian and ending in the Early Amazonian. No clear hiatus in eruptive activity is identified between these events, although a progression from eruptions at Syria Mons, to regionally distributed eruptions that form the bulk of the Syria Planum plains, to a final migration of dispersed eruptions to Syria's northwest is identified. Nearest neighbor analyses suggest a non-random distribution among the entire population of Syria Planum,

*Corresponding author. Department of Geology, University of South Florida, 4202 E. Fowler Ave. SCA528, Tampa, FL 33620. Tel. +1 813 974 8754
Email address: jrichardson@mail.usf.edu (Jacob A. Richardson)

which is interpreted as resulting from the interaction of independent magma bodies ascending through the crust during different stress regimes throughout the region's eruptive history. Two-point azimuth results identify three orientations of enhanced alignments, which match well with radial extensions of three major tectonic centers to the south, east, and northwest of the study area. As such, Syria Planum volcanism evolved from a central vent volcano to dispersed shield field development over several hundred million years, during which the independent magma bodies related to each small volcano interacted to some extent with one or more of at least three buried tectonic patterns in the older crust. These results show a strong relationship between independent mapping efforts of tectonic and volcanic features. Continued integration of volcano-tectonic mapping should provide direct constraints for future geodynamic models of magma production and thermal evolution of the Tharsis province.

Keywords:

Mars, Tharsis, Syria Planum, Volcanoes, Shields, Spatial statistics, Alignment statistics

¹ 1. Introduction

² The Tharsis province is a volcanic rise extending over 4500 km across the
³ western hemisphere of Mars, covering nearly a quarter of the planet's surface
⁴ (Hodges and Moore, 1994). This region is suggested to display volcanic and
⁵ tectonic activity into the late Amazonian (Anderson et al., 2001; Neukum
⁶ et al., 2004) (Martian chronology is detailed briefly in Section 2.3). The
⁷ region is long recognized to include five major shield volcanoes, seven partly

8 buried volcanoes, vast lava plains, and a wide range of smaller eruptive vents
9 (Carr et al., 1977; Greeley and Spudis, 1981; Mouginis-Mark et al., 1992;
10 Hodges and Moore, 1994). While twelve large named volcanoes are cataloged
11 and their morphologies and morphometries described in detail (Hodges and
12 Moore, 1994; Plescia, 2004, and references therein), small volcanic edifices
13 (10s km in diameter) have received much less attention due to a lack of high
14 resolution data with regional coverage prior to the Mars Global Surveyor
15 (MGS) mission.

16 The acquisition of post-*Viking* data enables for the first time detailed
17 cataloging and morphologic descriptions of the wide range of small volcanic
18 vents (hereafter referred to as small vents) in the Tharsis province (Baptista
19 et al., 2008; Baratoux et al., 2009; Bleacher et al., 2007, 2009; Brož and
20 Hauber, 2012; Hauber et al., 2009, 2011; Keszthelyi et al., 2008; Wilson
21 et al., 2009). This ability represents a critical step forward in the scientific
22 understanding of Martian magma production and eruption. Because different
23 types of volcanic features result from a combination of different eruptive
24 conditions, magma and lava properties, and ambient variables (Greeley, 1977;
25 Whitford-Stark, 1982), an understanding of the abundance and distribution
26 of volcanic features serves as a fundamental framework that is needed to fully
27 understand any volcanic system (Head et al., 1981; Connor and Conway,
28 2000).

29 Here we report on mapping and analyses of the vent fields within the
30 Syria Planum region of Mars (Baptista et al., 2008). This is a portion of
31 an ongoing investigation to catalog the location of small (10s km in diam-
32 eter) vents across the Tharsis region. Although each vent appears minor

33 in areal coverage and volume compared to the larger Tharsis shield volca-
34 noes, when considered together as vent fields comparable to the Snake River
35 Plain in Idaho, USA (Greeley, 1977, 1982), they represent significant magma
36 production events. In addition to the volume of lava visible on the surface,
37 the entire crust of the Tharsis region appears to have been demagnetized
38 (Connerney et al., 2005; Lillis, 2006). The passage of many small magma
39 packages into and through the crust provides a plausible explanation for this
40 demagnetization in areas that are hundreds of kilometers away from major
41 shield volcanoes (Lillis et al., 2009). Likewise, tectonic evidence has led to
42 the suggestion that the Tharsis province has experienced multiple episodes
43 of large mantle upwellings (Plescia and Saunders, 1982; Mege and Masson,
44 1996; Anderson et al., 2001, 2004; Wilson and Head, 2002), the centers of
45 which are not necessarily spatially overlapping with major volcanoes. An-
46 derson et al. (2001, 2004) refer to these events as magmatic-driven tectonic
47 episodes, which is consistent with the identification of vent fields in the Thar-
48 sis plains. As such, it is critical to assess the number, location, and duration
49 of magma production events that contributed to the current morphology of
50 the Tharsis region.

51 *1.1. Geologic Description*

52 Past mapping of Syria Planum has enabled the identification of several
53 distinct units based on morphologic characteristics. Baptista et al. (2008)
54 identified three distinct units in southwestern Syria: 1) a unit comprised
55 of NW-trending graben, 2) lava flows associated with Syria Mons, and 3)
56 a field of coalesced low shield volcanoes. The lava flows associated with
57 Syria Mons are hundreds of kilometers in length and form kilometers-wide,

58 finger-like sheets of lava throughout the unit. These flows embay the graben
59 field, which is composed of narrow (100s of meters to kilometers) linear and
60 curvilinear graben that are tens to hundreds of kilometers in length. The
61 Syria Mons flows are crosscut by NE-SW trending graben, 10s of km in
62 length. The coalesced shield field is composed of low shield volcanoes several
63 kilometers in diameter that embay the Syria Mons lava flows. Both the field
64 and the flows are crosscut with NW-SE trending graben (km in length). A
65 newly identified geologic unit (Hnsf in Figure 1) is located to the north of
66 the Baptista et al. (2008) study area and is seen to embay the coalesced
67 shield field to the south. It is characterized by lava flows tens to hundreds
68 of kilometers in length emanating from a topographic ridge approximately
69 200km in length that trends NE-SW. The lava flows that form this unit are
70 seen to fill preexisting graben that crosscut the southern coalesced shield field
71 and embay vents from the southern shield field.

72 The mapping of Baptista et al. (2008) was limited by High Resolution
73 Stereo Camera (HRSC) data availability to 100-105W, 13-23S within the
74 Syria region. Despite this limitation, Baptista et al. (2008) demonstrated
75 that analysis of high resolution image data with regional coverage showed
76 new volcanic and tectonic complexities in this region that had previously been
77 identified as a plains style volcanic province (Sakimoto et al., 2003) similar
78 to those described on the Earth (Greeley, 1982), and other Mars volcanic
79 field studies (Bleacher et al., 2007, 2009; Hauber et al., 2009). The addition
80 of several tectonic episodes that temporally separate volcanic emplacement
81 events leads to the hypothesis that Syria Planum is the surface product of
82 multiple (opposed to one long-lived) magma production events. For clarity,

83 we use the term “magma production event” to represent a broad magmatic
84 upwelling that might feed multiple shallow, crustal magma bodies and small
85 volcanic vents across a region like Syria. Such an event might be comparable
86 to an event that feeds a major shield like Olympus Mons or each of the
87 Tharsis Montes, and should be considered in models of the thermal and
88 geologic evolution of Tharsis. Therefore, it is imperative to determine if a
89 large field of vents like Syria represents one magma production event, or
90 possibly multiple, temporally distinct events that are spatially overlapping
91 on the surface of the planet.

92 In order to test this hypothesis we map volcanic vents in the full Syria
93 Planum region at comparable resolutions to the study of Baptista et al.
94 (2008), which is only now possible due to the combined data acquisition of
95 HRSC, Thermal Emission Imaging System (THEMIS), and Context Imager
96 (CTX) images. Our objectives are to determine if multiple separable magma
97 production events occurred in Syria and to assess whether these events can
98 be clearly identified as unique events or the extension of a long-lived, contin-
99 uous magma production event, either of which provide new insight into and
100 modeling constraints for the thermal and tectonic evolution of the Tharsis
101 province.

102 In this paper, new spatio-temporal boundaries of known volcanic units
103 are presented and a new volcanic unit in the north of Syria is identified,
104 separated from southern volcanism by a distinct flow margin. Each volcanic
105 unit in Syria Planum is temporally constrained with superposition relation-
106 ships and crater age-dating. Methods which are used to spatially describe
107 small volcanic vents in Syria are then discussed, including nearest neighbor

108 and 2-point azimuth statistical analyses. Finally, a revised volcano–tectonic
109 history of Syria Planum is proposed, wherein we interpret that volcanism has
110 likely migrated spatially throughout the evolution of Syria and wherein the
111 style of volcanism has likely shifted from one central vent at Syria Mons to
112 forming coalesced shield fields.

113 **2. Methods**

114 *2.1. Study Area*

115 The study area (Figure 1), Syria Planum, is located on the southeastern
116 margin of the Tharsis province between 8–23°S and 110–93°W. Syria Planum
117 is bordered by Noctis Labyrinthus to the north, Claritas Fossae to the west
118 and Solis Planum to the southeast. This area forms a regional plateau with
119 a maximum elevation of 8000 m based on analysis of Mars Orbiter Laser Al-
120 timeter (MOLA) (Smith et al., 2003) gridded data. A total relief of 4000 m
121 exists between this point and the southeastern portion of the study area. The
122 study area is roughly 1000 by 900 km in size as defined by Scott and Tanaka
123 (1986), with an abundance of volcanic vents focused in an area roughly 700 by
124 600 km in size (Richardson et al., 2010). In order to characterize the volcanic
125 evolution of Syria all identifiable volcanic vents in the study area are mapped
126 and morphologic units are identified as temporally separable by crater count-
127 ing. Nearest neighbor and 2-point azimuth statistical analyses are applied
128 to the vent location data to provide additional constraints on the evolution
129 of the volcanic region. A 512 pixels–per–degree (ppd) THEMIS infrared (IR)
130 day–time mosaic (Christensen et al., 2004) and the 128 ppd MOLA gridded
131 dataset (Smith et al., 2003) are used as base maps. Relevant CTX (Malin

¹³² et al., 2007) and THEMIS visible (VIS) (Christensen et al., 2004) images are
¹³³ co-registered to this base map for the identification of volcanic vents.

¹³⁴ *2.2. Catalog of Volcanic Vents*

¹³⁵ Volcanic vents are spatially cataloged as single points in a Cartesian grid,
¹³⁶ referencing their plan view position with respect to the THEMIS IR day–
¹³⁷ time mosaic and the gridded MOLA dataset base maps. Each datum is
¹³⁸ assumed to closely represent the four–dimensional (space and time) pathway
¹³⁹ along which magma ascended through the crust to erupt at the surface and
¹⁴⁰ produce an identifiable vent structure (Bishop, 2007). Volcanic vents are
¹⁴¹ here defined as positive topographic landforms, tens to hundreds of meters
¹⁴² in height, with flows or flow–like textures radiating from the apex and/or de-
¹⁴³ pressions at the topographic summit. Many positive topographic landforms
¹⁴⁴ lack clear flow features or a preserved depression at the apex, but are oth-
¹⁴⁵ erwise morphologically similar to cataloged vents. These landforms, which
¹⁴⁶ are tens to hundreds of meters in height, are also cataloged as likely volcanic
¹⁴⁷ vents (an example with contours is shown in Figure 1). It is assumed that
¹⁴⁸ many volcanic vents that formed within the volcanic field on Syria Planum
¹⁴⁹ have since been buried by continued volcanism. This mapping project does
¹⁵⁰ not consider these buried vents, nor does this study provide any assumptions
¹⁵¹ about stalled magma bodies for which ascension pathways were established
¹⁵² but did not lead to surface eruptions (in other words, the intrusion to extru-
¹⁵³ sion ratio of the region as was estimated in southern Tharsis by Lillis et al.
¹⁵⁴ (2009)). Instead, vents that are currently identifiable on the surface are as-
¹⁵⁵ sumed to represent the last stage of eruptive activity in the region and are
¹⁵⁶ used to provide new insight into the magmatic and volcanic history of Syria

157 and the Tharsis province.

158 A variety of volcanic vent morphologies are present on Tharsis and have
159 recently been characterized using post-*Viking* era image data (Bleacher et al.,
160 2007, 2009; Brož and Hauber, 2012; Keszthelyi et al., 2008; Baptista et al.,
161 2008; Hauber et al., 2009; Wilson et al., 2009; Baratoux et al., 2009). Different
162 methods are implemented for different vent morphologies to realistically
163 assign a representative two-dimensional point to this four-dimensional process.
164 For volcanic vents with depressions at the summit from which lava
165 has visibly erupted (based on interpretation of radiating textures or buildup
166 of spatter or cinder rims (examples in Figure 1)) a data point is digitally
167 created at the center of the depression using ArcGIS 9.3. For volcanic vents
168 with linear depressions along a topographic high, the data point is created
169 at the midpoint of a line with endpoints at the extents of the depression. In
170 cases where the depression extends beyond the apparent eruptive activity (in
171 other words, an extended dry fracture associated with the eruptive segment
172 of the fissure as discussed by Greeley (1977) in volcanic fields) the data point
173 is assigned at the middle point of a line connecting the ends of the eruptive
174 segment. For likely volcanic features, which do not display summit depressions,
175 data points were assigned at the topographic summit of the feature or
176 at the origin of radiating flow textures where possible.

177 Cataloging the location of volcanic vents within Syria also enables the
178 identification of distinct large scale flow features and units based on different
179 morphological and superposition characteristics. Consistent superposition
180 relationships among vent groups within Syria are identified. Using the
181 map of vent locations (Figure 1) and superposition relationships for Syria

182 Planum, several techniques are applied to further characterize the region's
183 eruptive history. Based on the identification of unique vent groups, crater
184 counts (described in Section 2.3) are conducted to test whether quantifiable
185 hiatuses occurred between the formation of different volcanic and tectonic
186 events. Nearest neighbor analysis (described in Section 2.4) is applied to the
187 complete Syria vent catalog and to subgroups of vents within the study area
188 based on morphological mapping units. Nearest neighbor analysis is applied
189 to assess the spatial distribution among vents. This has been shown as a
190 method of characterizing a group of data points as being composed of one
191 or a combination of populations (Bishop, 2007; Baloga et al., 2007). A two-
192 point azimuth technique (described in Section 2.5) is implemented to identify
193 potential lineaments between volcanic vents that might correlate to underly-
194 ing structures (Lutz, 1986; Wadge and Cross, 1988, 1989; Connor, 1990; Lutz
195 and Gutmann, 1995; Bleacher et al., 2009) in an attempt to better under-
196 stand the ascent of magma beneath Syria. The combination of such spatial
197 and alignment analyses has been used to characterize volcanic fields on the
198 Earth (Lutz, 1986; Lutz and Gutmann, 1995; Cebriá et al., 2011; Roberts
199 et al., 2011) and Mars (Bleacher et al., 2009).

200 *2.3. Crater Counting*

201 Using the 512ppd THEMIS infrared daytime mosaic, craters larger than
202 0.5 km are cataloged in accordance with identified vent groups and mor-
203 phologic units. For each morphologic unit, a crater retention age is fitted
204 to a cumulative crater size–frequency distribution following the method de-
205 scribed in Hartmann (2005) and using the freely available software Crater-
206 stats2 (Michael and Neukum, 2010). The size–frequency distribution is fit to

207 a production function from Ivanov (2001) and an absolute age is calculated
208 using the chronology model from Hartmann and Neukum (2001).

209 Given the relatively large surface area of each morphologic unit (e.g. one
210 unit is composed of >100 volcanic shields) and the relatively low spatial
211 resolution of the THEMIS mosaic (100 m), isochrons for this study are fit
212 using craters of diameter ≥ 1 km. Crater retention rates are reported with
213 errors following the equation

$$\text{214 } N(1) = \frac{n_{1km}}{A} \pm \frac{\sqrt{n_{1km}}}{A} \quad (1)$$

215 where n_{1km} is the observed number of craters with diameters greater than 1
216 km and A is the surface area in km^2 .

217 Ages determined by crater age-dating are assigned an epoch range based
218 on the Martian chronostratigraphic system as recently outlined by Werner
219 and Tanaka (2011). Generally, the three periods of the Martian system are
220 the Noachian, Hesperian, and Amazonian, ranging from >3.96-3.57 Ga, 3.57-
221 3.00 Ga, and 3.00 Ga-present, based on the chronology model of Hartmann
222 (2005), respectively. These periods are further separated into epochs as fol-
223 lows: Middle Noachian, 3.96-3.85 Ga; Late Noachian, 3.85-3.57 Ga; Early
224 Hesperian, 3.57-3.40 Ga; Late Hesperian, 3.40-3.00 Ga; Early Amazonian,
225 3.00-0.88 Ga; Middle Amazonian, 0.88-0.24 Ga; Late Amazonian, 0.24 Ga to
226 present.

227 2.4. Nearest Neighbor Analysis

228 The distances from each volcanic vent to its nearest neighboring vent in
229 a volcanic field can be used to characterize the spatial distribution of the
230 volcanic vents within a field. It has been hypothesized that the vents of a

231 terrestrial volcanic vent field (i.e. field volcanism) will conform to a random
232 spatial distribution (Lutz, 1986; Lutz and Gutmann, 1995). This is to say
233 that each vent is located in the study area independently of the location of
234 any other vent, that each vent has the same probability of occurrence at any
235 location in the study area, and that any subarea of the study area is equally
236 likely to contain any vent as any other identically sized study area (Clark
237 and Evans, 1954).

238 Based on the Poisson spatial distribution, Clark and Evans (1954) defined
239 two statistics with which to analyze nearest neighbor (NN) distances for a
240 spatial distribution of points. First, the test statistic, c , is given by the
241 equation

$$242 \quad c = \frac{\bar{r}_a - \bar{r}_e}{\sigma_e}, \quad (2)$$

243 where \bar{r}_a is the mean observed NN distance, \bar{r}_e is the expected mean NN
244 distance for a Poisson spatial distribution, and σ_e is the expected standard
245 deviation of NN distances. Expected values of c were simulated by Baloga
246 et al. (2007) to remove bias based on sample size. If the observed c statistic
247 departs from the expected c by more than 2σ for the appropriate sample size,
248 spatial randomness may be rejected.

249 Second, the ratio between the observed mean NN distance, \bar{r}_a , and the
250 expected mean NN distance, \bar{r}_e , given by equation 3, also tests the fit of
251 Poisson randomness.

$$252 \quad R = \frac{\bar{r}_a}{\bar{r}_e} \quad (3)$$

253 If a vent field is spatially random in a Poisson sense, the R -index will ap-
254 proach 1. Values of $R > 1$ suggest that the points approach maximal
255 packing, while values of $R < 1$ suggest that points are more clustered than

expected for a Poisson spatial distribution. Similar to the test statistic c , the calculated R -index may be compared to an expected $R \pm 2\sigma$ to test for the fit of Poisson randomness to describe the distribution of points.

Balog et al. (2007) also developed a test using the skewness and kurtosis of the NN distribution to further constrain the applicability of the Poisson distribution to a spatial sample. Using 1000 simulated Poisson point sets of the same sample size, it was observed that skewness and kurtosis are strongly correlated and focus around an elliptical centroid. If the skewness and kurtosis values for a given point set plot sufficiently far away from the centroid of simulated Poisson values, randomness in the Poisson sense may again be rejected.

Nearest neighbor analysis described above can be used to quantitatively compare the spatial distribution of volcanic vents with the null hypothesis, H_o , of spatial randomness in a Poisson sense. We hypothesize that if the vents are spatially random in the Poisson sense, then the vents have formed independently of each other as part of one larger magma production event (e. g. their respective magma ascension pathway through the crust was not influenced by the location of any other vent thereby causing a random spacing of eruption points). If a Poisson distribution is rejected and the R -index statistic shows evidence for clustering, we interpret the result as evidence that multiple temporally distinct magma production events have occurred beneath Syria Planum that are spatially overlapping, thereby resulting in two or more random but mixed statistical populations (Lutz, 1986; Lutz and Gutmann, 1995).

To perform nearest neighbor analysis, Geological Image Analysis Software

²⁸¹ (GIAS), version 1.12, was used (Beggan and Hamilton, 2010; Hamilton et al.,
²⁸² 2010, 2011).

²⁸³ *2.5. Two-point azimuthal analysis*

²⁸⁴ Two-point azimuth techniques have been used to observe and describe
²⁸⁵ lineaments between volcanic vents for decades (Lutz, 1986; Wadge and Cross,
²⁸⁶ 1988, 1989; Connor, 1990; Lutz and Gutmann, 1995; Bleacher et al., 2009;
²⁸⁷ Cebriá et al., 2011; Roberts et al., 2011). Azimuth techniques determine the
²⁸⁸ directions from each point to every other point. Lineaments between vents
²⁸⁹ are identified by looking at anomalously high numbers of azimuths in any
²⁹⁰ given direction and comparing that with other linear features, such as faults
²⁹¹ and graben, observed in the area or in adjacent, older terrains for which their
²⁹² traces might have been buried by the emplacement of the volcanic field or
²⁹³ other geologic processes.

²⁹⁴ Cebriá et al. (2011) postulated that lineaments between two vents are
²⁹⁵ more likely if those vents are relatively close to each other. They therefore
²⁹⁶ suggested that two point azimuth techniques should use a *minimum significant*
²⁹⁷ *distance*, a distance where the azimuths of closer inter-vent relationships
²⁹⁸ best characterize lineaments of the given field. Inter-vent relationships far-
²⁹⁹ ther than this minimum significant distance are not as likely to be related
³⁰⁰ by the same underlying geological structures. Adding to the benefit of using
³⁰¹ only inter-vent relationships smaller than this distance is that anomalously
³⁰² far inter-vent relationships will likely display bias in the direction of the vent
³⁰³ field's major axis. If the vent distribution for example, resembles a narrow
³⁰⁴ ellipse due to topographic focusing, the longer inter-vent relationships will
³⁰⁵ necessarily point in the direction of the long axis of the ellipse even if regional

306 tectonic patterns are perpendicular.

307 For this study, the minimum significant distance used is defined by Cebriá
308 et al. (2011)

309

$$d \leq (\mu_v - 1\sigma_v)/3 \quad (4)$$

310 where μ_v is the mean inter–vent distance and σ_v is the standard deviation
311 of inter–vent distances. Using the set of inter–vent relationships shorter
312 than this distance, relationships are grouped by direction into nine bins of
313 a rose diagram. We hypothesize that bins containing an anomalous amount
314 (count $\geq \bar{x}_n + \sigma_n$) of inter–vent relationships are evidence of lineaments
315 between vents. These orientations are compared with regional tectonic trends
316 as possible influences of magma ascension (Bleacher et al., 2009; Cebriá et al.,
317 2011).

318 **3. Results**

319 *3.1. Mapping*

320 In the study area 263 vents are identified, with 206 cataloged as volcanic
321 vents and 57 cataloged as likely volcanic vents. There is no specific area where
322 likely volcanic vents (as opposed to volcanic vents) are concentrated, though
323 the highest abundance of likely volcanic vents are in northern Syria Planum.
324 Because of the likely volcanic vents’ regional distribution and topographic
325 similarity to landforms cataloged as volcanic vents, we have included likely
326 volcanic vents in the statistical analysis of all volcanic vents on Syria Planum.
327 Here after both categories of vents are treated as one catalog, which includes
328 263 features.

329 The 263 identifiable vents within Syria Planum are distributed among five
330 of six identified map units on Syria, which are delineated based on observed
331 superposition relationships. Cataloged volcanic vents, geologic units, and
332 graben are plotted in Figure 1. A graben-rich unit previously described by
333 Baptista et al. (2008) and Tanaka and Davis (1988), Hg, is located in the
334 southwest of the study area and is seen to be embayed by the lavas of the
335 Syria Mons unit, Hsm. Lavas associated with Syria Mons cover much of the
336 study area and extend at least several hundreds of kilometers from Syria
337 Mons' main vent towards the southeast. The Syria Mons summit is the only
338 vent cataloged in this unit. The boundaries of the Syria Mons unit are defined
339 to the west and south by the margins of distinct, overlying lava flows. To
340 the east, the Syria Mons unit is embayed by low shields that coalesce into a
341 volcanic vent field, Hssf. Syria Mons and thirty volcanoes that make up this
342 coalesced vent field unit were extensively mapped by Baptista et al. (2008).
343 The majority of vents cataloged in Syria Planum, 192, are cataloged in this
344 vent field. Low shields that coalesce to form this unit have slopes 1-2.5° and
345 diameters between 10 and 35 kilometers. Eight vents are identified in this
346 unit that have slopes up to 6° and diameters of 2-10 km. The low shields
347 of this unit extend into the southeast where they flow over a unit of large
348 scale lava flows, Hlp, that extend from a center within Syria Planum, which
349 is unrecognized at this time. In this southeastern unit, 6 vents are cataloged.

350 To the north of the coalesced unit are distinct flow margins. The lava that
351 created these flow margins embay low shields associated with the coalesced
352 unit and fill graben that have cross-cut the coalesced unit. The source of
353 the embaying lava flows to the north is a unit comprised of 22 vents that

354 form a second coalesced volcanic vent field. To distinguish between these
355 two coalesced volcanic units, the field to the south, Hssf, is labeled as the
356 “southern shield field” and the field to the north, Hnsf as the “northern shield
357 field.” The northwestern boundary of the northern shield field is determined
358 by the extent of visible lava flows, which extend to the north and south of the
359 vents as far as 200 km. The northwest region of the study area is identified
360 as one unit, Hp, beyond the lava flows of Syria Mons and the northern shield
361 field. The northwestern unit contains 42 vents, which do not coalesce together
362 to make one distinct field. The relative superposition of this unit to the Syria
363 Mons lava flows and the northern shield field are not clearly defined.

364 The vents of the two coalesced shield fields are identified as subgroups
365 within the catalog of Syria Planum vents and are used for statistical analysis
366 in this study. The locations of volcanic vents cataloged in the study area
367 are summarized in Table 1. Because the flow fronts farthest from, but still
368 associated with, the northern shield field are buried by successive flow fronts
369 closer to the observed vents of the shield field, their temporal connection
370 to the observed vents is not confirmable. For this reason, geologically lower
371 flow fronts which are embayed by flows and are not able to be connected to
372 northern shield field vents are described as intermediate flows in age-dating
373 exercises discussed in Section 3.2.

374 *3.2. Age-Dating*

375 In Table 2 and illustrated graphically in Figure 2, crater counts and their
376 corresponding age-dates are presented. According to these counts, the last
377 lava flowed over the surface of Syria Planum as recent as the early Amazonian.
378 Crater dating also shows that the lavas from Syria Mons and the graben-

379 rich basement that they embay, which are the lowest observed geologic units,
380 were last significantly resurfaced during the early Hesperian epoch.

381 Using superposition, volcanic units are relatively dated with Syria Mons
382 erupting first, low shields of the southern shield field embaying its flows,
383 and lavas of the northern shield field embaying the southern shield field. As
384 shown in Figure 2, error bars between ages of flows associated with Syria
385 Mons, the southern shield field, and the northern shield field do not overlap
386 and are in agreement with superposition observations. However, no signifi-
387 cant haitus exists between the development of each unit. While some units
388 seem ambiguously dated with respect to superposition (e.g. the graben-rich
389 basement unit upon which are flows from Syria Mons is dated to be younger
390 than the Syria Mons flows), no unit is in direct disagreement with relative
391 dating observations, within error.

392 *3.3. Nearest Neighbor Analysis*

393 Figure 3 is a map of all vents cataloged in Syria Planum with lines drawn
394 to represent the connections from each vent to their nearest neighbor. Near-
395 est neighbor analysis is conducted using these distances. Table 3 presents
396 results of the nearest neighbor analyses. The first two columns of Table 3
397 give the expected and actual nearest neighbor distances for each area ex-
398 amined. The columns for R_e and c_e give the acceptance ranges for values
399 of R (defined in Equation 3) and c (defined in Equation 2), respectively,
400 based on sample size. The results of the skewness/kurtosis test are plotted
401 in Figure 4. Each plot shows simulated values of skewness and kurtosis for
402 1000 random Poisson spatial distributions (in gray). When the black dia-
403 mond (indicating actual skewness and kurtosis values) falls within the gray

404 area, this indicates consistency with Poisson randomness. Inferences based on
405 the skewness/kurtosis values shown in Figure 4 are summarized in the last
406 column of Table 3.

407 All cataloged vents in the study area are first analyzed as a single group to
408 test the null hypothesis, H_o , that the vents are spatially random in a Poisson
409 sense. Spatial randomness of the entire study area could be evidence that a
410 single magma production event may explain all volcanism on Syria Planum.
411 However, due to the low R -index, the low c statistic, and the result of the
412 skewness/kurtosis test where the field plotted outside the range of Poisson
413 randomness at the 99% confidence interval, we reject the null hypothesis that
414 the vents on Syria Planum are consistent with a Poisson spatial distribution
415 when the entire study area is considered. Moreover, the observed R -index
416 indicates that for all of Syria Planum the vents have a tendency to cluster,
417 which is evidence that multiple subgroups might be identified as independent
418 magma production events.

419 A subgroup that includes vents in both the northern and southern shield
420 fields is also examined. Nearest neighbor results of this subgroup (N & S
421 row in Table 3) inconclusively characterize the randomness of the combined
422 field. The observed c statistic is within the predicted range, the R -index is
423 calculated to be at the limit ($R = 1.11$) of the expected $R \pm 2\sigma$, and the
424 skewness and kurtosis values deviate from the elliptical centroid enough to
425 reject randomness at the 0.05 significance level.

426 The vents within the northern shield field and the southern shield field are
427 also analyzed individually to test their spatial randomness (Table 3). Accord-
428 ing to all three tests (the R -index, the c statistic, and the skewness/kurtosis

429 test) both the northern shield field and the southern shield field are found to
430 exhibit Poisson spatial randomness individually. Therefore the null hypoth-
431 esis of spatial randomness cannot be precluded for these shield fields. It is
432 important to note that the northern shield field includes only 22 vents, in-
433 creasing uncertainty in this conclusion. However, as the southern shield field
434 ($n = 192$) clearly exhibits spatial randomness and the combination of the two
435 shield fields produces an ambiguous spatial distribution, there is evidence to
436 suggest that the two shield fields are statistically distinct.

437 *3.4. Two-point azimuthal analysis*

438 Figure 6a displays a histogram of the lengths of all 34,453 inter–vent re-
439 lationships. The skewness of this set of distances is 0.79. The mean distance,
440 μ , is 267 km and the standard deviation, σ , is calculated to be 157 km. The
441 relationships used to investigate lineaments are below the minimum signif-
442 icant distance of ≤ 36.9 km as defined in Equation 4 (Cebriá et al., 2011).
443 The number of inter–vent relationships, n , below the minimum significant
444 distance, is 745. Figure 5 is a diagram of the vents represented as points in
445 two-dimensional Cartesian space, using their locations in meters, and rela-
446 tionships between vents that are below the minimum significant distance.

447 The rose diagram in Figure 6c illustrates the results of categorizing re-
448 lationships based on the direction. The mean quantity of relationships in
449 each direction bin, \bar{x}_n , is 82.8 and the standard deviation, σ_n , is 5.74. Three
450 bins are identified as containing heightened amounts (count $\geq \bar{x}_n + \sigma_n$) of
451 inter–vent relationships: 70-90° ENE, 350-10° N, and 310-330° NW.

452 A rose diagram (Figure 6b) has been included, which illustrates the 2–
453 point azimuth technique as applied to all inter–vent relationships, including

454 those above the minimum significant distance. The NW trend of the rela-
455 tionships is comparable to the NW trend of the overall vent field.

456 **4. Discussion**

457 Previous analyses of post-*Viking* era data show that the development of
458 the Syria Planum region can be subdivided into a series of tectonic and vol-
459 canic episodes. The goal of this study is to provide additional detail to this
460 sequence of events, and to determine if this region experienced one long-lived
461 magmatic event or a series of magma production events. Building upon the
462 work of Baptista et al. (2008) we present the following sequential volcano-
463 tectonic development for the Syria Planum region based on superposition
464 relationships. 1) Lava flows erupted from Syria Mons during the Early Hes-
465 perian (3.4-3.5 Ga), covering a recently (within hundreds millions of years)
466 formed graben-rich basement unit. 2) Northeast faulting cross-cut the Syria
467 Mons flows. 3) At 3.3-3.4 Ga during the Hesperian a southern shield field
468 formed through the eruption of small volcanic vents in central Syria Planum
469 to the NE of Syria Mons, which occurred contemporaneous to northwest
470 faulting in the region of the vent field. 4) Volcanism continued throughout
471 the northern region of Syria Planum from the Late Hesperian to the Early
472 Amazonian (2.9-3.3 Ga), while concentrating to create a northeast trending
473 ridge of coalesced vents north of and embaying the low shields of the southern
474 shield field.

475 The most noticeable addition to the work of Baptista et al. (2008) is the
476 separation of their coalesced shield field into a northern and southern coa-
477 lesced vent field for which the northern is younger based on superposition.

478 The delineation of two distinguishable vent fields in Syria, along with the
479 development of Syria Mons, reveals at least three significant volcanic units
480 or episodes. If these volcanic episodes all result from one magma production
481 event then they display a migration and evolution in eruptive style as Syria
482 volcanic units were emplaced through time. If not, then at least two, pos-
483 sibly more, magma production events produced the current surface of Syria
484 Planum and should be considered in models of the overall development of
485 the Tharsis province.

486 Crater counts of the units in this study (Table 2) are consistent with the
487 inferred relative ages of the units based on superposition as presented above.
488 Crater retention ages (Figure 2) suggest that currently preserved lavas flowed
489 across the Syria region as early as the Early Hesperian within the Syria Mons
490 unit and last flowed as recently as the Late Amazonian during emplacement
491 of the north field. We identify a slightly longer temporal range for volcanism
492 at Syria than Plescia (2004) and Baptista et al. (2008) possibly due to our
493 expanded mapping area and use of a more complete higher resolution set of
494 data. Regardless, our results indicate that volcanism at Syria likely spanned
495 a period of time no longer than \sim 900 Ma. However, we also note that Hauber
496 et al. (2011) conducted crater counts of select individual vents within Syria
497 Planum, finding that some small shields might have erupted as recently as
498 several hundred million years ago. Although our crater counts do not sug-
499 gest significant temporal overlaps between the volcanic units, error bars do
500 terminate against one another. As such, crater counts confirm our sequential
501 inferences, but are inconclusive, taken on their own, with regard to differen-
502 tiating between multiple and a single magma production event related to the

503 emplacement of Syria Planum lava flows.

504 The application of spatial and alignment statistical analyses to vent lo-
505 cation data within monogenetic vent fields on the Earth have previously
506 enabled researchers to identify unique vent populations within a field and
507 their relationships to regional tectonics (Connor and Conway, 2000, e.g.).
508 Although such results are often supported by extensive field work, Bishop
509 (2007) showed the value of conducting such analyses based on remote sensing
510 data alone, and recently researchers have demonstrated the potential for us-
511 ing those analyses on martian vent fields (Bishop, 2008; Bleacher et al., 2009;
512 Hamilton et al., 2010, 2011). The Nearest Neighbor and 2–Point Azimuth
513 analyses used here are based on decades of terrestrial research supported by
514 field work and are used here to provide additional insight into the devel-
515 opment of Syria Planum where mapping and crater counting alone cannot
516 adequately test our hypothesis.

517 Lutz (1986) and Lutz and Gutmann (1995) suggest that vent fields with
518 nonrandom spatial distributions represent an overlap of more than one pop-
519 ulation of randomly spaced vents. Nearest Neighbor analyses for the entire
520 Syria Planum vent field yields a non-random spatial distribution of vents.
521 Based on our mapping that delineates a northern and southern shield field in
522 Syria Planum, and the work of Lutz (1986) and Lutz and Gutmann (1995),
523 we interpret this result to indicate that at least two populations of vents
524 with unique spatial signatures make up the Syria Planum region. Together,
525 the vents of these fields yield a nearest neighbor result of questionable con-
526 sistency with a random Poisson distribution, but removal of the northern
527 field from the southern field yields a result clearly consistent with a random

528 Poisson distribution for the southern field (Table 3). As such, our geologic
529 interpretation of the random statistical spacing of these features is that the
530 southern shield field represents one unique population of volcanic vents. The
531 spacing of 22 vents in the northern shield field is also consistent with a ran-
532 dom distribution. One interpretation of these Nearest Neighbor results is
533 the existence of more than one magma production event, each identified by
534 a randomly sorted population of vents in the study area. Another interpre-
535 tation of Syria's overall nonrandom vent spacing is that magmatic activity
536 migrated towards the north where magma ascension might have been con-
537 trolled by different tectonic influences that affected the spacing dynamics
538 of the subsequently emplaced vent field. The Nearest Neighbor results are
539 consistent with the possibility of more than one magma production event, in
540 contrast with age-dating results, which do not identify any detectable hia-
541 tus in eruptive activity during the entirety of the observable volcanic history
542 of Syria Planum. In spite of this contrast, we are able to confidently state
543 that the southern field is representative of a significant magma production
544 event. The addition of the northern field vents to the southern field vents con-
545 fuses those results: a clear distinction between two magma production events
546 (southern *and* northern) and a single evolving event (southern *to* northern)
547 is not found.

548 Many terrestrial volcanic fields display migrations in activity throughout
549 the eruptive cycle associated with a major magma production event. The
550 Springerville Volcanic Field, AZ, is perhaps one of the best examples of
551 this process. Monogenetic volcanism of Springerville was active from Late
552 Pliocene to Holocene (2.1 to 0.3 Ma), producing basaltic low shields and

553 cinder cones. Over the course of its volcanic activity, vent formation migrated
554 eastward by roughly 2.5 cm/yr. A compositional progression is also seen:
555 volcanism erupted tholeiitic basalts early on and changed over time to erupt
556 alkalic olivine basalts (Condit et al., 1989, 1999).

557 The results of two-point azimuth analysis for Syria reveal three predom-
558 inant trends of vent alignment centered at 0°, 80°, and 320° from north
559 (Figure 6). We interpret the geologic cause of these alignments to be shal-
560 low faulting which constrained the placement of small vents. Most clearly,
561 northwest faulting first observed by Baptista et al. (2008) occurred contem-
562 poraneously to the formation of the south field, which corresponds to the
563 observed northwest vent alignment. Additionally, while the faulting pattern
564 in the graben-rich basement unit trends NW, specifically trending between
565 330-350° which corresponds to a paucity of inter-vent alignments (Figure 6),
566 it is possible that faulting continues and shifts direction where this base-
567 ment unit is buried. East-west trending graben are observed in the north-
568 west region of the study area extending from the western margins of Noctis
569 Labyrinthus towards the northern shield field, which might correspond to
570 the vent alignments observed at 80°. Such a tectonic influence on magma
571 ascension later in the development of the Syria Planum, particularly in the
572 north, might have caused the confused Nearest Neighbor results discussed
573 above. The alignment of vents to the north is not supported by faulting that
574 is observable at the surface. This might provide insight into the possibility
575 of buried regional-scale faults with north-south alignments.

576 This mapping project enables insight into the origin of Syria Mons and
577 its relationship to the coalesced field of shields to the east and north. The

mapping presented here and by Baptista et al. (2008) demonstrates that Syria Mons is comparable to other large Tharsis shield volcanoes in areal extent, although with a much lower relief than Olympus Mons and the Tharsis Montes. Does Syria Mons itself represent a unique magma production event that is distinct from the coalesced shields? Superposition demonstrates a consistent embayment of Syria Mons by flows associated with the coalesced vent field. However, crater count data again cannot be used to rule out the possibility of synchronous eruptions within these two units as their error bars end against each other. It is not uncommon for terrestrial shield volcanoes to experience a dispersal of eruption sites in the late stages of volcano growth. This is perhaps best observed at Mauna Kea, Hawaii. As Hawaiian shield volcanoes transition from the tholeiitic shield building to alkali capping stages the eruptions become less frequent and produce shorter flows (Moore and Mark, 1992; Wolfe and Morris, 1996; Rowland and Garbeil, 2000; Bleacher and Greeley, 2008). This transition is the result of numerous effects primarily related to a decrease in magma delivery rate to the surface as the volcano is pulled away from the consistently active Hawaiian hotspot due to plate tectonics. This decrease in magma supply is no longer capable of sustaining a primary shallow magma reservoir at the older volcanoes like occurs at Kilauea or Mauna Loa, and as a result each eruption represents an isolated package of magma. Because these eruptions do not share a shallow magma source they each find their own way to the surface and the eruption sites are dispersed across the volcano. Like the decreased magma supply rate at Mauna Kea, a decrease in the magma supply rate under Syria Mons might have caused a similar dispersal of eruption sites from one central vent volcano

603 to a series of independent vents. Coupled with changing regional stress fields
604 that are displayed by different fault orientations throughout Syria Planum,
605 it might be possible for one major magma production event under the Syria
606 region to have evolved from a sustained central vent edifice (Syria Mons)
607 to plains-style, coalesced vent field volcanism that itself migrated from the
608 southeast to northwest of Syria.

609 Comparison of the vent spatial and alignment data with the tectonic
610 history of the region yields additional insight into the sequential development
611 of Syria. Syria Planum, and the surrounding areas, are identified as long
612 standing centers of tectonic activity with major tectonic centers existing 1)
613 between Syria and Claritas Fossae in the Noachian, 2) along the southern-
614 central portion of Valles Marineris in the Late Noachian and Early Hesperian,
615 and 3) northwest of Syria into the Early Hesperian (Dohm and Tanaka, 1999;
616 Anderson et al., 2001, 2004) (See Figure 7). Dohm and Tanaka (1999) suggest
617 that these tectonic centers likely resulted from significant volcano-tectonic
618 activity, and likely produced much of the volcanic deposition that is seen in
619 those regions today.

620 Comparison of our detailed analyses of the volcanic features within Syria
621 to the tectonic evolution of Tharsis highlights some unique commonalities.
622 The tectonic history suggests a change in location and decrease in intensity of
623 tectonic activity towards the northeast across the Syria region from Claritas
624 Fossae to Valles Marineris, then westward across the northern extent of the
625 Syria region between the Noachian and Early Hesperian (Dohm and Tanaka,
626 1999; Anderson et al., 2002; Anderson et al., 2004). Volcanism in Syria,
627 as revealed in this study, migrated east away from Syria Mons, and subse-

628 quently to the northwest between Early Hesperian and Early Amazonian.
629 This migration was coupled with an evolution from one major central vent
630 volcano, to broadly distributed volcanism that formed many, smaller central
631 vent volcanoes whose flow fields coalesced to completely resurface Syria. This
632 style of volcanic evolution (single central vent to broadly distributed vents)
633 is also associated, at least in part, with a waning magma supply on some
634 terrestrial volcanoes (Moore and Mark, 1992; Wolfe and Morris, 1996; Row-
635 land and Garbeil, 2000; Bleacher and Greeley, 2008). It is not clear at what
636 time Syria Mons volcanism began. Dohm and Tanaka (1999) suggest that
637 Noachian volcanism from the Syria region emplaced some of the basement
638 units that were later deformed during the formation of Claritas Fossae and
639 Webb et al. (2001) suggest that these eruptions built up the Syria Planum
640 topographic rise by the Late Noachian to Early Hesperian as a major vol-
641 canic center that was > 2000 km in diameter and displaying at least 8 km of
642 relief.

643 A coupled tectonic history of Tharsis and volcanic evolution of Syria is
644 presented here. During the Noachian a center of province-wide tectonism
645 was located between Syria and Claritas Fossae, essentially south of the study
646 area. At this time extensive volcanic plains units were emplaced between
647 Syria and the Thaumasia region to the south, for which no known vents
648 are currently exposed at the surface in Syria. Tectonism at this time would
649 have created radial crustal fractures that trended north through the study
650 area, which is one of three orientations of heightened inter-vent relationships
651 identified in the two-point azimuth analysis (Figure 6). Between the Late
652 Noachian and Early Hesperian the center of Tharsis tectonism shifted north-

653 eastward towards Valles Marineris. At the same time volcanism in Syria
654 evolved into a single central vent volcano, Syria Mons, although we cannot
655 rule out the possibility of additional distributed volcanic centers across Syria
656 that are now covered by younger deposits. At this time the tectonic center
657 was located to the east of Syria and would have created west trending crustal
658 structures through the study area, which again is an orientation of heightened
659 inter–vent relationships in Syria (Figure 6). During the Early Hesperian, as
660 tectonism continued to shift, now towards the west/northwest, volcanism
661 evolved into dispersed development of numerous small volcanic centers that
662 were distributed across several hundred kilometers of the Syria region. Tec-
663 tonism related to this center would have created southeast trending crustal
664 structures across the study area at this time, which is the orientation of the
665 third heightened inter–vent relationship orientations identified in this study
666 (Figure 6). Following the Early Hesperian, tectonism was focused far to the
667 north near Alba Patera. Volcanism in Syria declined through the Hesperian
668 and eventually ended sometime in the Early Amazonian.

669 5. Conclusion

670 Mapping of the Syria Planum region of Mars shows at least 263 volcanic
671 vents ranging in diameter from one volcano > 100 km (Syria Mons) to most
672 volcanoes at 10s of km. Mapping, crater counts, and spatial and alignment
673 statistical analyses reveal a complex volcano–tectonic history for this region
674 that represents at least one major magma production event in the develop-
675 mental history of Tharsis.

676 Mapping of lava flows and vents, and their superposition relationships

677 shows a sequence of volcanic activity from a broad shield volcano, Syria
678 Mons, in the early Hesperian to a coalesced field of individually, areally
679 smaller shields that together resurfaced much of the region through the Late
680 Hesperian, possibly including the shields in northwest Syria. This broadly
681 distributed activity eventually became focused to form a northeast trending
682 topographic ridge composed of the region's youngest group of small shield
683 volcanoes into the Early Amazonian. Crater counts support these mapping-
684 based inferences, indicating that each stage of activity followed the previous
685 stage with no significant hiatus and that each stage likely lasted between 60
686 and 650 Ma. Spatial statistics are inconclusive with regard to differentiating
687 multiple events, but do suggest that the earlier coalesced shield field and
688 the northern ridge shield field each represent a unique randomly distributed
689 group of vents. We interpret this result to indicate that each group's vents
690 formed by the ascension and eruption of isolated magma bodies and did not
691 share a common shallow magma reservoir for which magma scavenging of
692 shared resources might have affected vent location.

693 Results from the study of Syria Planum tectonism and volcanism highlight
694 the difficulty of identifying unique magma production events across planetary
695 volcanic provinces for which detailed field work is not possible. It is assumed
696 that major shield volcanoes on Mars might be related to magma production
697 events similar to the concept of mantle plumes in terrestrial geology. How-
698 ever, the cause of eruptions for shield field volcanism across such large areas
699 of the Martian crust are more difficult to interpret. Our remote sensing-
700 based mapping, crater counts, and spatial and alignment analyses do not
701 conclusively demonstrate either that Syria experienced one, evolving magma

702 production event, or a series of unique events that are spatially overlapping.
703 However, the tectonic evolution around and across Syria does demonstrate
704 that the Syria region was influenced by evolving stress fields during the same
705 frame of time that volcanic eruptions were occurring. We identify orienta-
706 tions of enhanced inter-vent alignments that are aligned with extensions of
707 all three of the closest tectonic centers through our study area. Although
708 buried, these structural features within the underlying crust of Syria appear
709 to have influenced the ascension of magma bodies to the surface between the
710 Early Hesperian and Early Amazonian, as is seen for the field of volcanic
711 vents south of Pavonis Mons (Bleacher et al., 2009).

712 It is clear that the Syria Planum region is a major center of Tharsis vol-
713 canism, and that this volcanic center is surrounded by at least three major
714 tectonic centers, which appear to have influenced the locations of vent forma-
715 tion across Syria. The mapped distribution (both spatially and temporally)
716 of volcanism in the region can be used to provide direct constraints for testing
717 various hypotheses on the internal processes such as geodynamical models of
718 melt generation from mantle convection (O'Neill et al., 2007, e.g.) and/or
719 lithospheric delamination (Scott and Wilson, 2003, e.g.). Although we can-
720 not identify unique volcanic stages that are temporally isolated by eruptive
721 hiatuses, we do identify the development of two unique units of coalesced
722 small shields. The emplacement of these two shield fields occurred over a
723 period of 100–800 Ma, both following the development a major central vent
724 volcano. When taken as a whole, the entire region evolved from a central vent
725 volcano into a dispersed volcanism across ∼900 Ma. Our future work focuses
726 on determining the volumes of lava erupted during these volcanic events as

727 an additional modeling constraint. Continued mapping of surface features
728 should provide direct constraints for future integrated geodynamic models
729 of volcanic and tectonic processes that were related to significant Tharsis
730 province magma production events.

731 **6. Acknowledgments**

732 Funding for this project was provided to all three authors by NASA's Mars
733 Data Analysis Program. Additional support for J. Richardson was provided
734 by NASA's Undergraduate Student Research Program funding through God-
735 dard Space Flight Center. We thank Nick Schmerr for insightful comments
736 that improved the content of this report.

737 **7. References**

- 738 Anderson, R.C., Dohm, J.M., Golembek, M.P., Haldemann, A.F.C.,
739 Franklin, B.J., Tanaka, K.L., Lias, J., Peer, B., 2001. Primary centers and
740 secondary concentrations of tectonic activity through time in the western
741 hemisphere of Mars. *Journal of Geophysical Research* 106, 20,563–20,585.
- 742 Anderson, R.C., Dohm, J.M., Haldemann, A.F.C., Hare, T., 2002. Com-
743 parative Investigation of the Geological Histories Among Alba Patera and
744 Syria Planum, Mars, in: Lunar and Planetary Institute Science Conference
745 Abstracts, p. 1811.
- 746 Anderson, R.C., Dohm, J.M., Haldemann, A.F.C., Hare, T.M., Baker, V.R.,
747 2004. Tectonic histories between Alba Patera and Syria Planum, Mars.
748 *Icarus* 171, 31–38.

- 749 Baloga, S.M., Glaze, L.S., Bruno, B.C., 2007. Nearest-neighbor analysis of
750 small features on Mars: Applications to tumuli and rootless cones. *Journal*
751 of Geophysical Research
- 112, E03002.
- 752 Baptista, A.R., Mangold, N., Ansan, V., Baratoux, D., Lognonné, P., Alves,
753 E.I., Williams, D.A., Bleacher, J.E., Masson, P., Neukum, G., 2008. A
754 swarm of small shield volcanoes on Syria Planum, Mars. *Journal of Geo-*
755 *physical Research* 113, E09010.
- 756 Baratoux, D., Pinet, P., Toplis, M.J., Mangold, N., Greeley, R., Baptista,
757 A.R., 2009. Shape, rheology and emplacement times of small martian
758 shield volcanoes. *Journal of Volcanology and Geothermal Research* 185,
759 47–68.
- 760 Beggan, C., Hamilton, C.W., 2010. New image processing software for ana-
761 lyzing object size-frequency distributions, geometry, orientation, and spa-
762 tial distribution. *Computers & Geosciences* 36, 539–549.
- 763 Bishop, M., 2007. Point pattern analysis of eruption points for the Mount
764 Gambier volcanic sub-province: a quantitative geographical approach to
765 the understanding of volcano distribution. *Area* 39, 230–241.
- 766 Bishop, M., 2008. Higher-order neighbor analysis of the Tartarus Colles cone
767 groups, Mars: The application of geographical indices to the understanding
768 of cone pattern evolution. *Icarus* 197, 73–83.
- 769 Bleacher, J.E., Glaze, L.S., Greeley, R., Hauber, E., Baloga, S.M., Sakimoto,
770 S.E.H., Williams, D.A., Glotch, T.D., 2009. Spatial and alignment analyses
771 for a field of small volcanic vents south of Pavonis Mons and implications

- 772 for the Tharsis province, Mars. *Journal of Volcanology and Geothermal*
773 *Research* 185, 96–102.
- 774 Bleacher, J.E., Greeley, R., 2008. Relating volcano morphometry to the
775 developmental progression of Hawaiian shield volcanoes through slope and
776 hypsometric analyses of SRTM data. *Journal of Geophysical Research* 113,
777 B09208.
- 778 Bleacher, J.E., Greeley, R., Williams, D.A., Cave, S.R., Neukum, G., 2007.
779 Trends in effusive style at the Tharsis Montes, Mars, and implication for
780 the development of the Tharsis province. *Journal of Geophysical Research*
781 112, E09005.
- 782 Brož, P., Hauber, E., 2012. A unique volcanic field in Tharsis, Mars: Pyro-
783 clastic cones as evidence for explosive eruptions. *Icarus* 218, 88 – 99.
- 784 Carr, M.H., Greeley, R., Blasius, K.R., Guest, J.E., Murray, J.B., 1977. Some
785 Martian volcanic features as viewed from the Viking orbiters. *Journal of*
786 *Geophysical Research* 82, 3985–4015.
- 787 Cebriá, J.M., Martín-Escorza, C., López-Ruiz, J., Morán-Zenteno, D.J., Mart-
788 tiny, B.M., 2011. Numerical recognition of alignments in monogenetic vol-
789 canic areas: Examples from the Michoacán-Guanajuato Volcanic Field in
790 Mexico and Calatrava in Spain. *Journal of Volcanology and Geothermal*
791 *Research* 201, 73–82.
- 792 Christensen, P., Jakosky, B., Kieffer, H., Malin, M., McSween, H., Neal-
793 son, K., Mehall, G., Silverman, S., Ferry, S., Caplinger, M., Ravine, M.,

- 794 2004. The Thermal Emission Imaging System (THEMIS) for the Mars
795 2001 Odyssey Mission. *Space Science Reviews* 110, 85–130.
- 796 Clark, P.J., Evans, F.C., 1954. Distance to Nearest Neighbor as a Measure
797 of Spatial Relationships in Populations. *Ecology* 35, 445–453.
- 798 Condit, C.D., Crumpler, L.S., Aubele, J.C., 1999. Lithologic, Age Group,
799 Magnetopolarity, and geochemical maps of the Springerville Volcanic
800 Field, East-Central Arizona. USGS Miscellaneous Investigations Series
801 Map I-2431.
- 802 Condit, C.D., Crumpler, L.S., Aubele, J.C., Elston, W.E., 1989. Patterns
803 of Volcanism along the Southern Margin of the Colorado Plateau: The
804 Springerville Field. *Journal of Geophysical Research* 94, 7975–7986.
- 805 Connerney, J.E.P., Acuna, M.H., Ness, N.F., Kletetschka, G., Mitchell, D.L.,
806 Lin, R.P., Reme, H., 2005. Tectonic implications of Mars crustal mag-
807 netism. *Proceedings of the National Academy of Science* 102, 14,970–
808 14,974.
- 809 Connor, C.B., 1990. Cinder Cone Clustering in the TransMexican Volcanic
810 Belt: Implications for Structural and Petrologic Models. *Journal of Geo-*
811 *physical Research* 95, 19,395–19,405.
- 812 Connor, C.B., Conway, M.F., 2000. Basaltic volcanic fields, in: Sigurdsson,
813 H. (Ed.), *Encyclopedia of Volcanoes*. Academic Press, San Diego, CA, pp.
814 331–343.
- 815 Dohm, J.M., Tanaka, K.L., 1999. Geology of the Thaumasia region, Mars:

- 816 plateau development, valley origins, and magmatic evolution. *Planetary*
817 and *Space Science* 47, 411 – 431.
- 818 Greeley, R., 1977. Basaltic “plains” volcanism, in: Greeley, R., King, J.S.
819 (Eds.), *Volcanism of the Eastern Snake River Plain, Idaho: A Comparative*
820 *Planetary Geology Guidebook*, NASA CR-154621. NASA, Washington, D.
821 C., pp. 23–44.
- 822 Greeley, R., 1982. The Snake River Plain, Idaho: Representative of a new
823 category of volcanism. *Journal of Geophysical Research* 87, 2705–2712.
- 824 Greeley, R., Spudis, P.D., 1981. Volcanism on Mars. *Reviews of Geophysics*
825 and *Space Physics* 19, 13–41.
- 826 Hamilton, C.W., Fagents, S.A., Thordarson, T., 2011. Lavaground ice in-
827 teractions in Elysium Planitia, Mars: Geomorphological and geospatial
828 analysis of the Tartarus Colles cone groups. *Journal of Geophysical Re-*
829 *search* 116, E03004.
- 830 Hamilton, C.W., Fagents, S.A., Wilson, L., 2010. Explosive lava-water in-
831 teractions in Elysium Planitia, Mars: Geologic and thermodynamic con-
832 straints on the formation of the Tartarus Colles cone groups. *Journal of*
833 *Geophysical Research* 115, E09006.
- 834 Hartmann, W.K., 2005. Martian cratering 8: Isochron refinement and the
835 chronology of Mars. *Icarus* 174, 294 – 320.
- 836 Hartmann, W.K., Neukum, G., 2001. Cratering chronology and
837 the evolution of Mars. *Space Science Reviews* 96, 165–194.
838 doi:10.1023/A:1011945222010.

- 839 Hauber, E., Bleacher, J., Gwinner, K., Williams, D., Greeley, R., 2009. The
840 topography and morphology of low shields and associated landforms of
841 plains volcanism in the Tharsis region of Mars. *Journal of Volcanology*
842 and *Geothermal Research* 185, 69–95.
- 843 Hauber, E., Brož, P., Jagert, F., Jodłowski, P., Platz, T., 2011. Very recent
844 and wide-spread basaltic volcanism on Mars. *Geophysical Research Letters*
845 38, L10201.
- 846 Head, J.W., Bryan, W.B., Greeley, R., Guest, J.E., Shultz, P.H., Sparks,
847 R.S.J., Walker, G.P.L., Whitford-Stark, J.L., Wood, C.A., Carr, M.H.,
848 1981. Basaltic volcanic fields, in: W. M. Kaula, et al. (Ed.), *Basaltic*
849 *Volcanism on the Terrestrial Planets*. Pergamon Press Inc., New York, pp.
850 702–887.
- 851 Hodges, C.A., Moore, H.J., 1994. *Atlas of Volcanic Landforms on Mars*,
852 USGS Prof. Paper 1534. U. S. Govt. Printing Office, Washington, D. C.
- 853 Ivanov, B.A., 2001. Mars/Moon Cratering Rate Ratio Estimates. *Space*
854 *Science Reviews* 96, 87–104.
- 855 Keszthelyi, L., Jaeger, W., McEwen, A., Tornabene, L., Beyer, R.A., Dun-
856 das, C., Milazzo, M., 2008. High Resolution Imaging Science Experiment
857 (HiRISE) images of volcanic terrains from the first 6 months of the Mars
858 Reconnaissance Orbiter Primary Science Phase. *Journal of Geophysical*
859 *Research* 113, E04005.
- 860 Lillis, R., 2006. Electron reflectometry as a probe of the Martian crust and
861 atmosphere, doctoral thesis. Department of Physics, UC Berkeley.

- 862 Lillis, R.J., Dufek, J., Bleacher, J.E., Manga, M., 2009. Demagnetization of
863 crust by magmatic intrusion near the Arsia Mons volcano: Magnetic and
864 thermal implications for the development of the Tharsis province, Mars.
865 Journal of Volcanology and Geothermal Research 185, 123–138.
- 866 Lutz, T.M., 1986. An Analysis of the Orientations of Large-scale Crustal
867 Structures:A Statistical Approach Based on Areal Distributions of Point-
868 like Features. Journal of Geophysical Research 91, 421–434.
- 869 Lutz, T.M., Gutmann, J.T., 1995. An improved method for determining and
870 characterizing alignments of pointlike features and its implications for the
871 Pinacate volcanic field, Sonora, Mexico. Journal of Geophysical Research
872 100, 17,659–17,670.
- 873 Malin, M.C., Bell, J.F., Cantor, B.A., Caplinger, M.A., Calvin, W.M.,
874 Clancy, R.T., Edgett, K.S., Edwards, L., Haberle, R.M., James, P.B.,
875 Lee, S.W., Ravine, M.A., Thomas, P.C., Wolff, M.J., 2007. Context Cam-
876 era Investigation on board the Mars Reconnaissance Orbiter. Journal of
877 Geophysical Research 112, E05S04.
- 878 Mege, D., Masson, P., 1996. A plume tectonics model for the Tharsis
879 Province, Mars. Planetary and Space Science 44, 1499–1546.
- 880 Michael, G., Neukum, G., 2010. Planetary surface dating from crater size-
881 frequency distribution measurements: Partial resurfacing events and sta-
882 tistical age uncertainty. Earth and Planetary Science Letters 294, 223 –
883 229.

- 884 Moore, J.G., Mark, R.K., 1992. Morphology of the Island of Hawaii. GSA
885 Today 2, 257–262.
- 886 Mouginis-Mark, P.J., Wilson, L., Zuber, M.T., 1992. The physical volcanol-
887 ogy of Mars, in: H. H. Kieffer, et al. (Ed.), Mars. The University of Arizona
888 Press, Tucson, pp. 424–452.
- 889 Neukum, G., Jaumann, R., Hoffmann, H., Hauber, E., Head, J.W.,
890 Basilevsky, A.T., Ivanov, B.A., Werner, S.C., van Gasselt, S., Murray,
891 J.B., McCord, T., TeamThe, H.R.S.C.I.C., 2004. Recent and episodic vol-
892 canic and glacial activity on Mars revealed by the High Resolution Stereo
893 Camera. Nature 432, 971–979.
- 894 O'Neill, C., Lenardic, A., Jellinek, A.M., Kiefer, W.S., 2007. Melt propa-
895 gation and volcanism in mantle convection simulations, with applications
896 for Martian volcanic and atmospheric evolution. Journal of Geophysical
897 Research 112, E07003+.
- 898 Plescia, J.B., 2004. Morphometric properties of Martian volcanoes. Journal
899 of Geophysical Research 109, E03003.
- 900 Plescia, J.B., Saunders, R.S., 1982. Tectonic history of the Tharsis region,
901 Mars. Journal of Geophysical Research 87, 9775–9791.
- 902 Richardson, J.A., Bleacher, J.E., Baptista, A.R., 2010. Identification of Vol-
903 canic Ridge in Northern Syria Planum, Mars: Constraint on Geologic
904 History of Syria, in: Lunar and Planetary Institute Science Conference
905 Abstracts, p. 1427.

- 906 Roberts, K.S., Davies, R.J., Stewart, S.A., Tingay, M., 2011. Structural
907 controls on mud volcano vent distributions: examples from Azerbaijan
908 and Lusi, east Java. *Journal of the Geological Society* 168, 1013–1030.
909 <http://jgs.lyellcollection.org/content/168/4/1013.full.pdf+html>.
- 910 Rowland, S.K., Garbeil, H., 2000. Slopes of oceanic basalt volcanoes, in:
911 P. J. Mouginis-Mark, et al. (Ed.), *Remote Sensing of Active Volcanism*,
912 *Geophys. Monogr. Ser.*. AGU, Washington, D. C.. volume 116.
- 913 Sakimoto, S.E.H., Gregg, T.K.P., Hughes, S.S., Chadwick, J., 2003. Re-
914 Assessing Plains-style Volcanism on Mars, in: A. L. Albee & H. H. Kieffer
915 (Ed.), *Sixth International Conference on Mars*, p. 3197.
- 916 Scott, D.H., Tanaka, K.L., 1986. Geologic map of the Western Equatorial
917 region of Mars. USGS Miscellaneous Investigations Series Map I1802A.
- 918 Scott, E., Wilson, L., 2003. Did the Alba Patera and Syria Planum regions of
919 Mars lose their lithospheric roots in convective overturn events? *Journal*
920 *of Geophysical Research* 108, 5035+.
- 921 Smith, D.E., Zuber, M.T., Neumann, G.A., Guinness, E.A., Slavney, S.,
922 2003. Mars Global Surveyor Laser Altimeter Mission Experiment Gridded
923 Data Record. NASA Planetary Data System, MGS-M-MOLA-5-MEGDR-
924 L3-V1.0.
- 925 Tanaka, K.L., Davis, P.A., 1988. Tectonic History of the Syria Planum
926 Province of Mars. *Journal of Geophysical Research* 93, 14,893–14,917.
- 927 Wadge, G., Cross, A., 1988. Quantitative methods for detecting aligned

- 928 points: An application to the volcanic vents of the Michoacan-Guanajuato
929 volcanic field, Mexico. *Geology* 16, 815–818.
- 930 Wadge, G., Cross, A.M., 1989. Identification and analysis of the alignments
931 of point-like features in remotely-sensed imagery. *Volcanic cones in the*
932 *Pinacate Volcanic Field, Mexico. International Journal of Remote Sensing*
933 *10*, 455–474.
- 934 Webb, B., Head, III, J.W., Kortz, B.E., Pratt, S., 2001. Syria Planum, Mars:
935 A Major Volcanic Construct in the Early History of Tharsis, in: *Lunar and*
936 *Planetary Institute Science Conference Abstracts*, p. 1145.
- 937 Werner, S., Tanaka, K., 2011. Redefinition of the crater-density and absolute-
938 age boundaries for the chronostratigraphic system of Mars. *Icarus* 215, 603
939 – 607.
- 940 Whitford-Stark, J.L., 1982. Factors influencing the morphology of volcanic
941 landforms: An Earth-Moon comparison. *Earth Science Reviews* 18, 109–
942 168.
- 943 Wilson, L., Head, J.W., 2002. Tharsis-radial graben systems as the sur-
944 face manifestation of plume-related dike intrusion complexes: Models and
945 implications. *Journal of Geophysical Research* 107, 5057.
- 946 Wilson, L., Mouginis-Mark, P.J., Tyson, S., Mackown, J., Garbeil, H., 2009.
947 Fissure eruptions in Tharsis, Mars: Implications for eruption conditions
948 and magma sources. *Journal of Volcanology and Geothermal Research*
949 *185*, 28–46.

950 Wolfe, E.W., Morris, J., 1996. Geologic map of the Island of Hawaii, scale
951 1:100,000. USGS Miscellaneous Investigations Series Map I-2524-A.

Table 1: Summary of Vent Counts in Defined Units

	Volcanic Vents	Likely Volcanic Vents	Total Vents
Northern Shield Field, <i>Hnsf</i> ^a	13	9	22
Southern Shield Field, <i>Hssf</i> ^a	159	33	192
Syria Mons Unit, <i>Hsm</i>	1	0	1
Northwest Syria Planum, <i>Hp</i>	28	14	42
Southeast Syria Planum, <i>Hlp</i>	4	2	6
Totals	205	58	263

^a Nearest neighbor analysis is performed on the vent populations of the northern and southern shield fields and the combination of these fields.

Table 2: Crater Retention Rates and Ages for Selected Units

	10^{-3} N(1) craters km $^{-2}$	Age, Ga	Epoch ^a
Northern Shield Field, <i>Hnsf</i>	1.4 ± 0.2	2.56-3.23	Late Hesp. to Early Amaz.
Northwest Syria Planum, <i>Hp</i>	1.5 ± 0.1	3.17-3.29	Late Hesp.
Intermediate Flows, <i>Hnsf?</i>	1.7 ± 0.4	3.28-3.52	Early to Late Hesp.
Southern Shield Field, <i>Hssf</i>	1.7 ± 0.1	3.23-3.35	Late Hesp.
Southeast Syria Planum, <i>Hlp</i>	1.8 ± 0.1	3.33-3.40	Late Hesp.
Syria Mons Unit, <i>Hsm</i>	2.0 ± 0.1	3.41-3.47	Early Hesp.
Graben Basement, <i>Hg</i>	2.2 ± 0.2	3.37-3.46	Early to Late Hesp.

^a Hesp.: Hesperian; Amaz.: Amazonian.

Table 3: Summary of Nearest Neighbor Analysis on Cataloged Vents and two Subgroups of Vents

	\bar{r}_e	\bar{r}_a	R_e	R	c_e	c	S/K plot
All Syria Planum	18.7 km	16.5 km	1.03 ± 0.07	0.88	0.80 ± 2.14	-3.57	rejected
N&S Shield Fields	13.6 km	14.7 km	1.03 ± 0.08	1.11	0.82 ± 2.14	2.20	rejected
Southern Shield Field	13.6 km	15.4 km	1.03 ± 0.09	1.09	0.83 ± 2.15	2.29	accepted
Northern Shield Field	14.9 km	12.3 km	1.15 ± 0.39	1.25	0.97 ± 2.57	1.82	accepted

\bar{r}_e , the expected mean NN distance; \bar{r}_a , the observed mean NN distance; R_e , the expected R -index and acceptance range; R , the observed R -index value (from Equation 3); c_e , the expected c statistic and acceptance range; c , the observed c statistic (from Equation 2). The final column lists the results of the skewness/kurtosis plot tests, testing the null hypothesis of Poisson spacing at the 0.05 significance level.

Table 4: Notation

c	test statistic for spatial randomness.
\bar{r}_a	observed mean Nearest Neighbor distance.
\bar{r}_e	expected mean Nearest Neighbor distance.
σ_e	expected standard deviation of Nearest Neighbor distances.
R	index comparing \bar{r}_a and \bar{r}_e to test spatial randomness.
d	minimum significant distance of 2-point azimuth analysis.
μ_v	mean inter–vent distance.
σ_v	standard deviation of inter–vent distances.
\bar{x}_n	mean quantity of inter–vent relationships in directional bins.
σ_n	standard deviation of inter–vent relationships in directional bins.

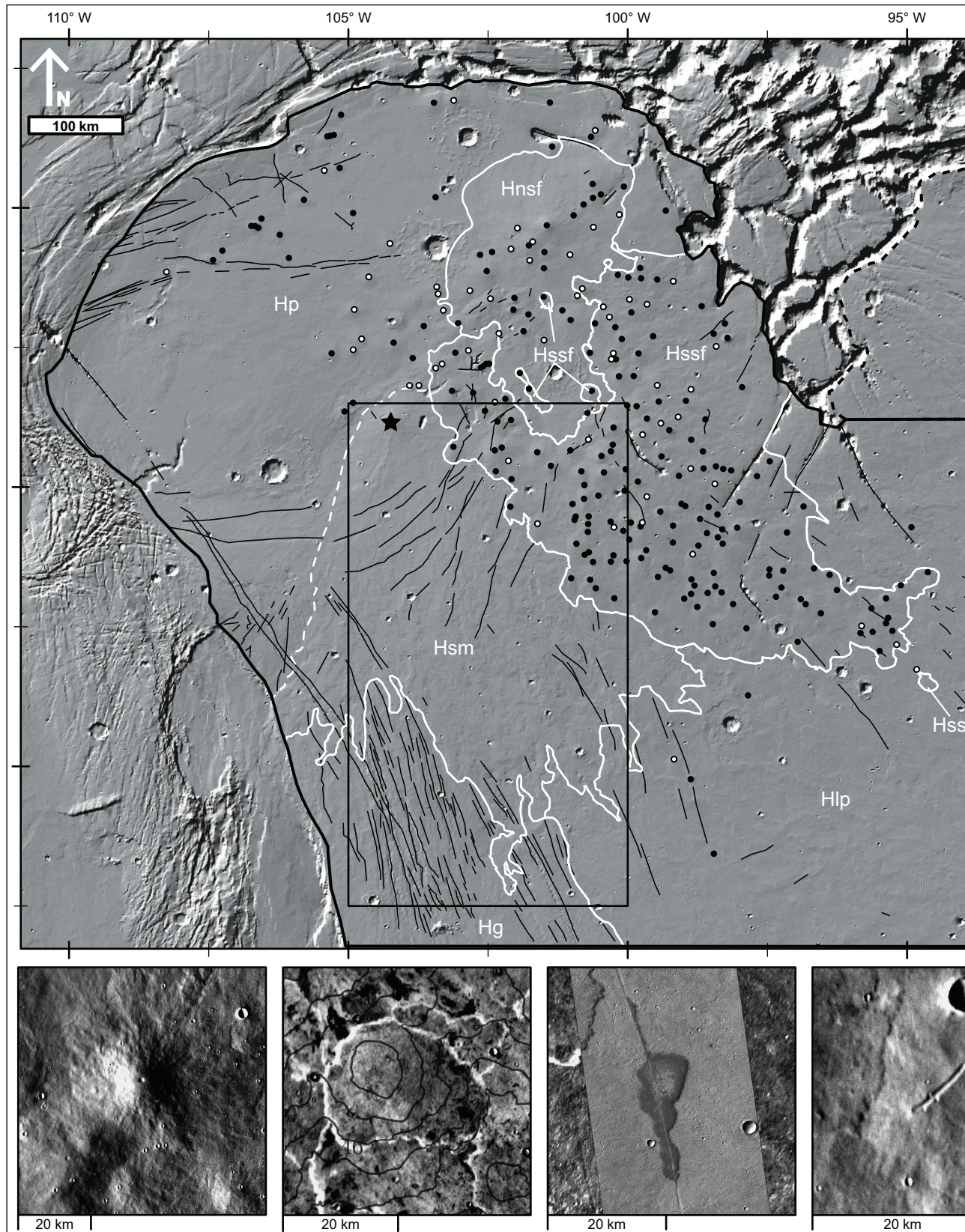


Figure 1: Geologic Map of Syria Planum. The study area is shown inside the thick black line with a MOLA-derived hillshade basemap. The study area of Baptista et al. (2008) is

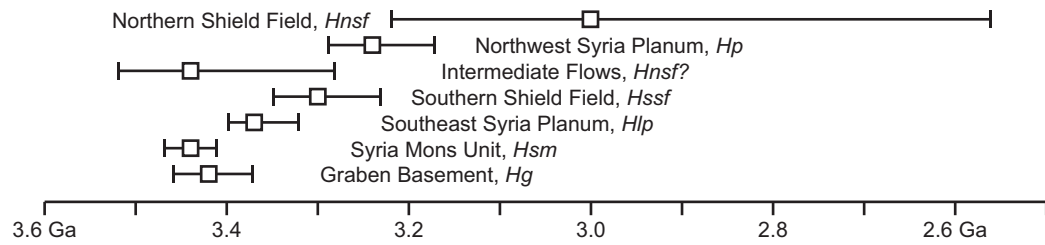


Figure 2: Graphical summary of age-dating results by unit.

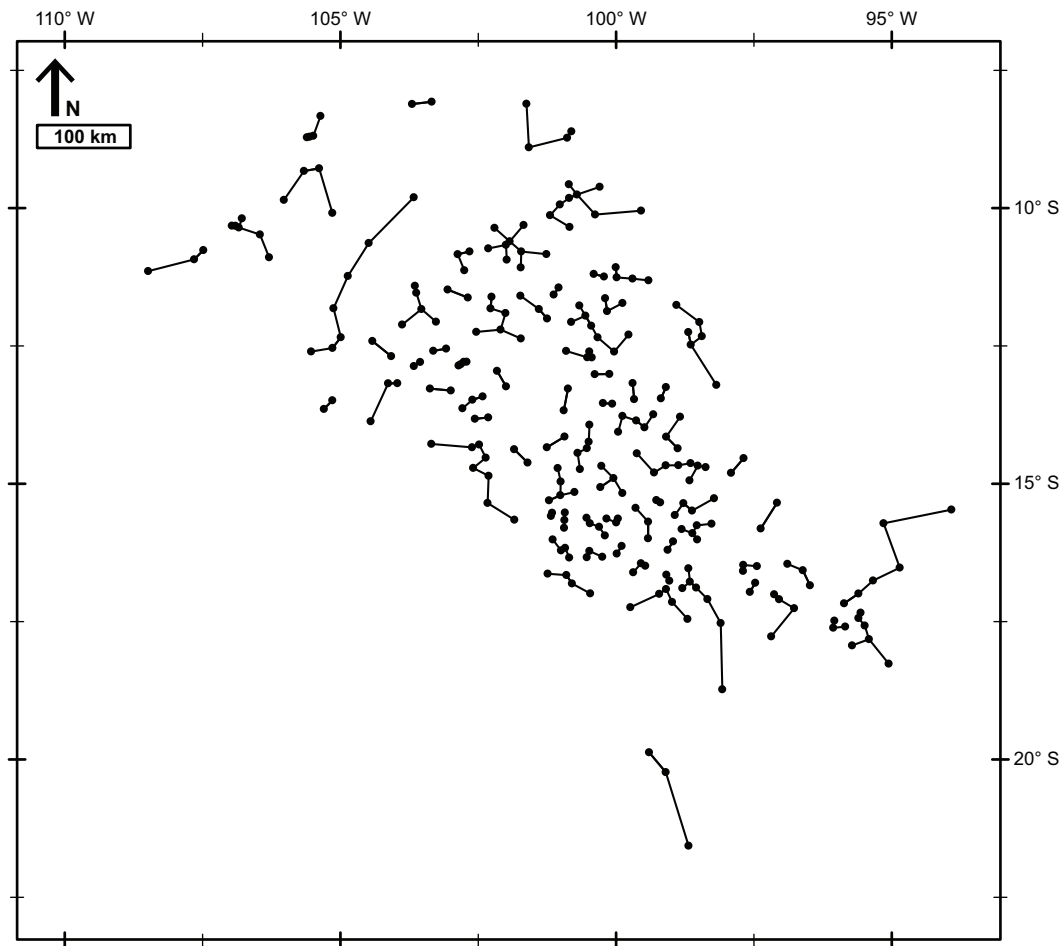


Figure 3: Plot of vents with lines drawn to their nearest neighbors.

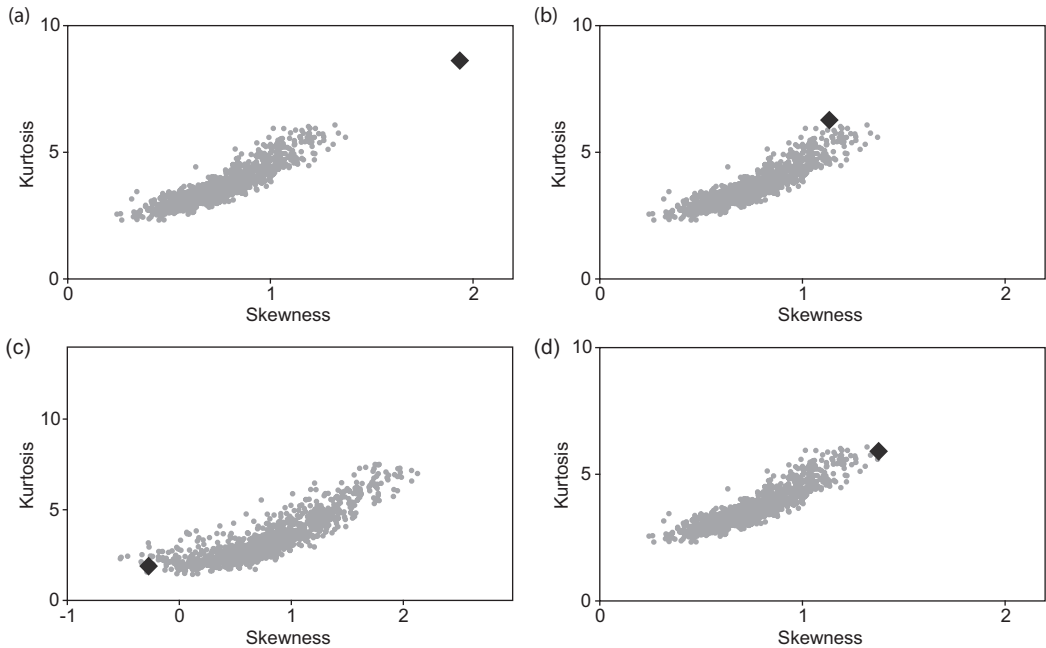


Figure 4: Plots of skewness vs. kurtosis values for 95% of 1000 simulated Poisson spatial distributions. Diamonds represent the corresponding experimental values for a) all cataloged vents on Syria Planum, b) vents in both shield fields, c) vents in the northern shield field, and d) vents in the southern shield field. Randomness is rejected for all vents and for the combined shield fields (a, b respectively) at the 0.05 significance interval and accepted for both shield fields (c,d) individually. Simulated Poisson spatial distributions for a, b, and d use 300 data points; for c, 30 data points.

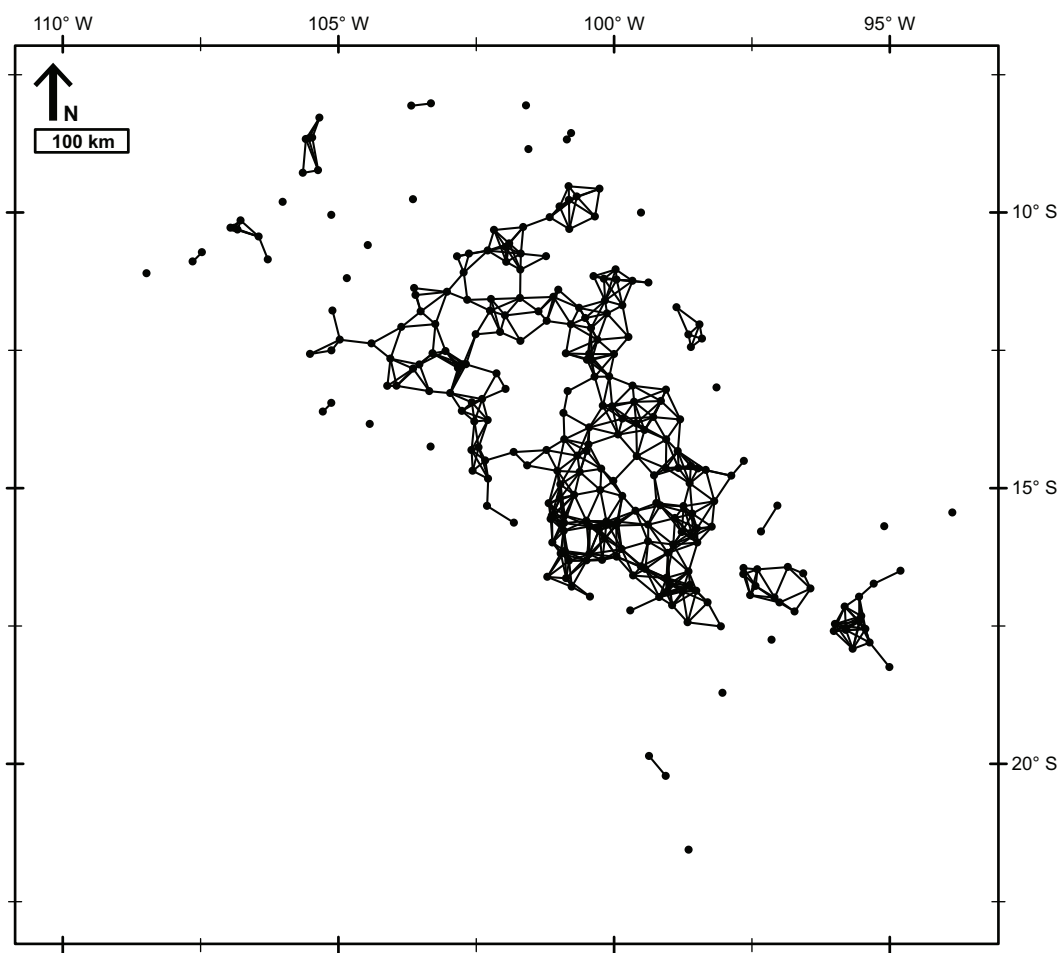


Figure 5: Plot of vents and all inter-vent relationships less than the minimum significant distance.

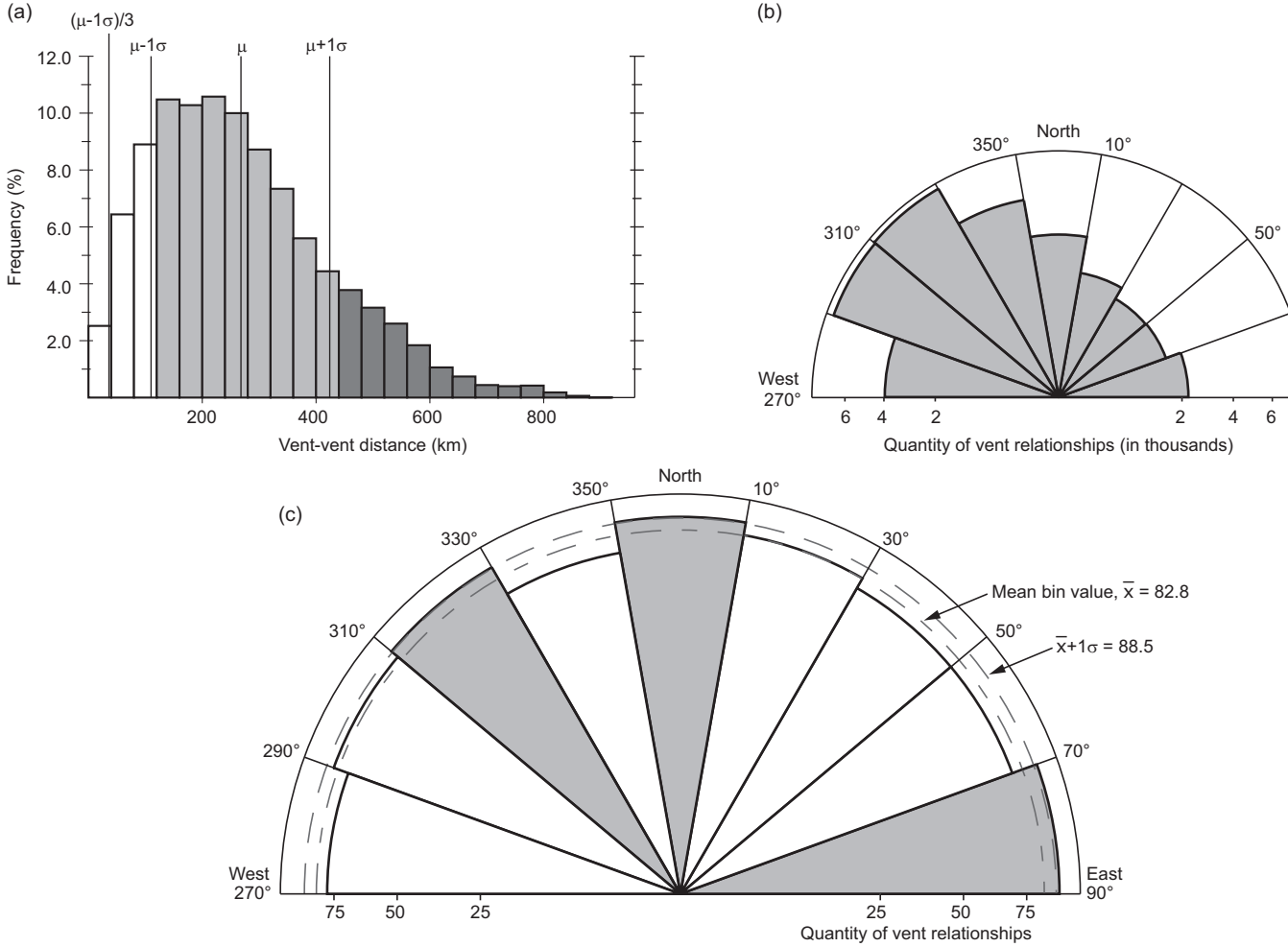


Figure 6: a) Distribution of inter-vent distances. Azimuths of inter-vent relationships are used if the inter-vent distance is less than 39.6 km, the defined minimum significant distance. Distances shaded dark gray are anomalously long and might trend in the overall vent field. Distances shaded light gray are of moderate length and are considered to be background noise. b) Directional distribution considering all inter-vent relationships. The plotted northwest mode is a result of including long distance inter-vent relationships. c) Directional distribution of inter-vent alignments below the minimum significant distance. The inner dotted line represents the mean quantity of inter-vent relationships. The outer dotted line represents the quantity of relationships one standard deviation above the mean. Directional wedges shaded gray ($70-90^\circ$, $310-330^\circ$, $350-10^\circ$) have anomalously high quantities of inter-vent relationships.

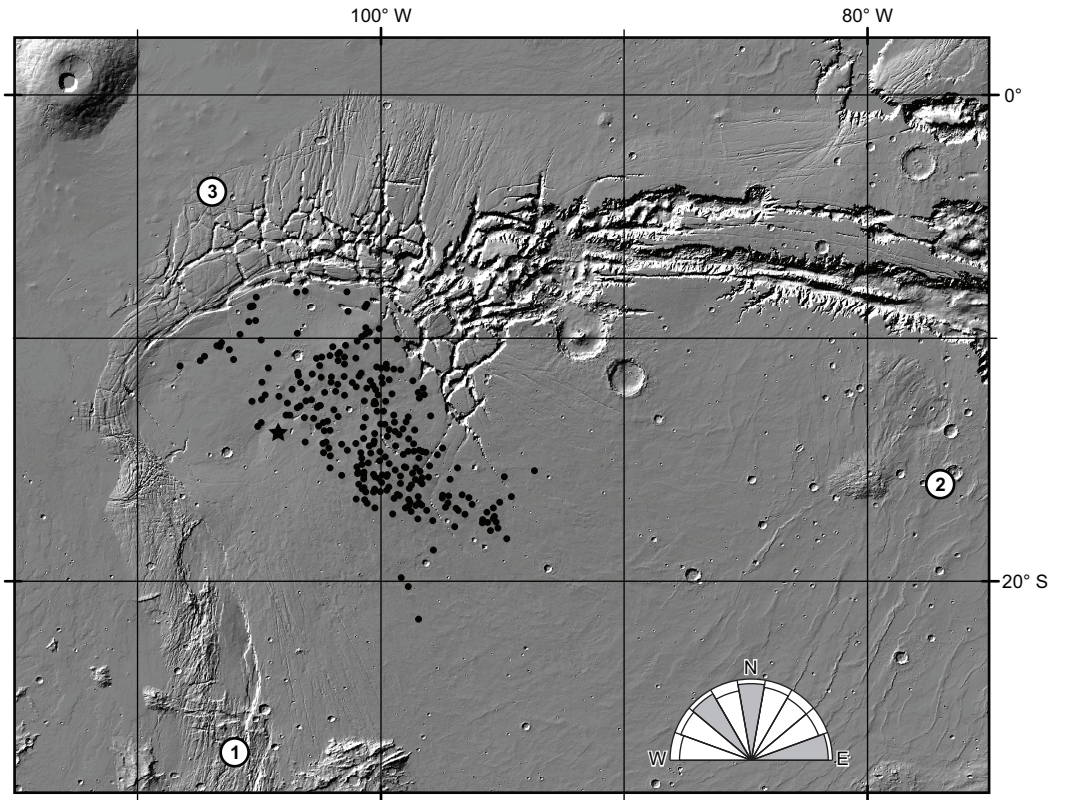


Figure 7: Anderson et al. (2001) described tectonic centers located at numbered circles: 1) between Syria and Claritas Fossae in the Noachian, 2) along the southern-central portion of Valles Marineris in the Late Noachian and Early Hesperian, and 3) northwest of Syria into the Early Hesperian. Black circles: vents in this study; star: Syria Mons. The rose diagram of Figure 6c is reproduced in the bottom right to illustrate similarities between inter-vent alignments and directions between Syria Planum and tectonic centers.